Bifurcation analysis of a multi-transverse-mode VCSEL

Kirk Green[a] and Bernd Krauskopf[b]

[a]Department of Theoretical Physics, Vrije Universiteit, De Boelelaan 1081, 1081HV Amsterdam, The Netherlands

[b]Department of Engineering Mathematics, University of Bristol, Bristol BS8 1TR, UK

ABSTRACT

We study the behaviour of a multi-transverse-mode vertical-cavity surface-emitting laser subject to optical feedback in which the optical modes are coupled through the external round-trip. Starting from a delayed partial differential equation description of the spatial optical mode profiles and the carrier diffusion, we first use eigenfunction expansion techniques to resolve the spatial dependence. The resulting system of delay differential equations is then amenable to a full nonlinear bifurcation analysis by means of numerical continuation techniques. As illustration, we present bifurcation diagrams of a two-mode VCSEL in the plane of feedback strength versus feedback phase. In this way, we identify a number of changes in the structure and bifurcations of the VCSEL's dynamics. In particular, we find coexisting stable steady state solutions, which bifurcate to stable in-phase and anti-phase periodic solutions with vastly differing frequencies. We show how these periodic solutions give rise to quasiperiodic and chaotic laser dynamics.

Keywords: Semiconductor laser, optical feedback, optical mode coupling, eigenfunction expansion, numerical continuation, anti-phase dynamics, chaos

1. INTRODUCTION

In this paper we investigate a vertical cavity surface emitting laser (VCSEL) subject to optical feedback from an external mirror. We start from a general partial differential equation (PDE) description of the VCSEL[1–4] that describes the interplay between the spatial optical modes, competing for the same reservoir of carriers; there is both spatial and temporal competition between the modes. The first step in our analysis is to resolve the spatial nature of the governing system. In the past, this has typically involved the use of a Fourier series expansion in the rotational, azimuthal direction, followed by a finite difference discretisation in the radial direction.[3] However, the resulting system is generally quite large, and may be hard to deal with numerically.[5] In this study we employ eigenfunction expansion techniques to both the azimuthal direction and the radial direction.[6] In this way, the PDE is reduced to a set of ordinary differential equations of a reasonable size. Our next step is to include the effect of optical feedback. This results in a delay differential equation (DDE) description. The final DDE model is amenable to a full nonlinear bifurcation analysis with tools such as `DDE-BIFTOOL`[7] and `PDDE-CONT`,[8] as well as being more computationally efficient when using standard time integration techniques.

When modelling a VCSEL subject to optical feedback, pure self-feedback is normally assumed;[3,9] that is, each spatial mode only influences itself after the external round-trip. However, in reality this is not necessarily the case. For example, modes may couple through deformities in the mirror. Furthermore, orthogonality of these modes is lost in the far-field, resulting in a non-zero overlap between them. Therefore, we consider a model in which general coupling via the external feedback is included.[5] More specifically, in this study, we investigate the effect of changing the feedback strength and feedback phase on the stability of a VCSEL for which the two fields couple roughly equally into each other after the external round-trip. We identify regions of multistability between coexisting solutions and show how steady operation may be destabilised into two different periodic regimes. Namely, we find in-phase dynamics on the frequency of undamped relaxation oscillations, and anti-phase dynamics on the timescale of the external cavity round-trip time. We finish by showing how these solutions bifurcate to more complicated quasiperiodic and chaotic dynamics.

E-mail addresses: k.green@few.vu.nl, b.krauskopf@bristol.ac.uk

2. RATE EQUATIONS

A VCSEL can be described by the following system of dimensionless PDEs:[2–5]

$$\frac{dE^j_{mn}(t)}{dt} = (1+i\alpha)\xi^j_{mn}(t)E^j_{mn}(t) + F^j_{mn}(t), \tag{1}$$

$$\begin{aligned} T\frac{\partial N(r,\phi,t)}{\partial t} &= \frac{d_f}{r}\left[\frac{\partial}{\partial r}\Big(r\frac{\partial N(r,\phi,t)}{\partial r}\Big)\right] + \frac{d_f}{r^2}\frac{\partial^2 N(r,\phi,t)}{\partial \phi^2} + P(r,\phi,t) - N(r,\phi,t) \\ &- \sum_n \Bigg((1+2\xi_{0n}(t))|E_{0n}(t)|^2 |\Psi_{0n}(r,\phi)|^2 \\ &\qquad + \sum_m \sum_{j=c,s} 2(1+2\xi^j_{mn}(t))|E^j_{mn}(t)|^2 |\Psi^j_{mn}(r,\phi)|^2 \Bigg) \end{aligned} \tag{2}$$

for the evolution of the slowly varying complex electric field $E^j_{mn}(t)$ of the mnth linearly polarised mode in its jth polarisation and the spatial carrier population $N(r,t,\phi)$. The associated profiles of the linearly polarised modes are given by $\Psi^j_{mn}(r,\phi)$; they are solutions of a scalar wave equation.[2–6] The function $F^j_{mn}(t)$ describes an external perturbation, for example, optical injection or feedback, applied to the optical fields. The spatial pump $P(r,\phi,t) \equiv P(r)$ is described by a disc-shaped contact over the core region of the VCSEL, with a maximum value of $P_{\max} = 2$. In the study that follows, other material parameters are fixed at values of the linewidth enhancement factor $\alpha = 3$, the ratio between electron and photon lifetimes $T = 750$, and a diffusion coefficient $d_f = 0.05$. The modal gains ξ^j_{mn} are given by integrals describing the spatial overlap between the respective optical field and the inversion; see Ref. [6] for full details. (In order to interpret the temporal dynamics physically, note that time is rescaled with respect to the photon lifetime $\tau_p = 2$ ps.)

To make Eqs. (1) and (2) amenable to a full nonlinear bifurcation analysis we must first resolve their spatial dependence. As is common,[3] we first deal with the azimuthal dependence by using a Fourier series expansion

$$N(r,\phi,t) = \sum_{k=0}^{\infty} \big(N_{ck}(r,t)cos(k\phi) + N_{sk}(r,t)sin(k\phi) \big). \tag{3}$$

To resolve the radial dependence we could use a finite difference discretisation scheme.[3,5] However, this typically results in a large-scale system of differential equations. Therefore, we chose to perform a second expansion (in suitable eigenfunctions). Namely we use a kth order Bessel function expansion[6]

$$N_k(r,t) = \sum_{q=1}^{\infty} N_{kq}(t) J_k(\gamma_{k,q} r). \tag{4}$$

After these expansions, and suitable orthogonality conditions have been applied, we are left with a general spatially resolved system describing a multi-transverse-mode VCSEL.[6]

In this paper we only consider the first two rotationally symmetric modes LP_{01} and LP_{02}. Their three-dimensional profiles $\psi_1 = |\Psi_1|^2$ and $\psi_2 = |\Psi_2|^2$ are shown in Fig. 1. These modes are obtained by assuming that the cold-cavity VCSEL takes the form of a cylindrical waveguide; see Refs. [2–6] for full details. Two-mode VCSELs have been studied experimentally in Ref. [10]. Theoretical studies of the two-mode VCSEL can be found in Refs. [5, 9]. In this case, the rate equations (1)–(2) reduce to

$$\frac{dE_1(t)}{dt} = (1+i\alpha)\xi_1 E_1(t) + \kappa e^{iC_p}\big[\eta E_1(t-\tau) + (1-\eta)E_2(t-\tau)\big], \tag{5}$$

$$\frac{dE_2(t)}{dt} = (1+i\alpha)\xi_2 E_2(t) + \kappa e^{iC_p}\big[\eta E_2(t-\tau) + (1-\eta)E_1(t-\tau)\big], \tag{6}$$

$$T\frac{dN_q(t)}{dt} = -(\gamma^2_{0,q} d_f + 1)N_q(t) + \rho_q - \sum_{n=1}^{2}\left((1+2\xi_n)|E_n(t)|^2 \beta^{0q}_n \right); \tag{7}$$

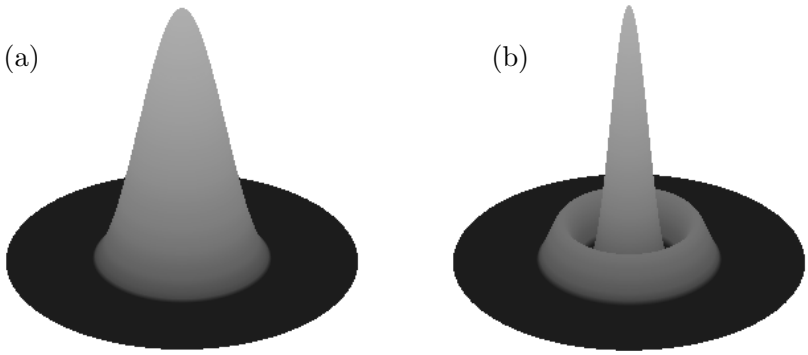

Figure 1. Normalised spatial profiles $|\Psi_1(r,\phi)|^2$ and $|\Psi_2(r,\phi)|^2$ of the linearly polarised modes LP_{01} (a) and LP_{02} (b).

which is a set of $q+4$ equations. We consider here a total of $q=14$ expansion terms, that is, a total system of size 18. (The relative error at the steady state solutions between a system with $q=14$ and one with $q=100$ was found to be less than 0.01%). The overlap integrals, which need to be evaluated only once, are now given as

$$\xi_n = \sum_{q=1}^{14} \int_0^1 \Big(|\Psi_n(r)|^2 N_q J_0(\gamma_{0,q} r) \Big) r dr, \tag{8}$$

$$\rho_q = \frac{2}{[J_1(\gamma_{0,q})]^2} \int_0^1 P(r) J_0(\gamma_{0,q} r)\, r dr, \tag{9}$$

$$\beta_n^{0q} = \frac{2}{[J_1(\gamma_{0,q})]^2} \int_0^1 |\Psi_n(r)|^2 J_0(\gamma_{0,q} r)\, r dr. \tag{10}$$

Moreover, we have explicitly introduced in Eqs. (5)–(7) an external perturbation in the form of optical feedback.[11] Specifically, the feedback enters with a common feedback strength κ and feedback phase C_p. The delay time is set to $\tau = 500$, which corresponds to a distance of approximately 10 cm between the laser and the mirror. The homotopy parameter η represents the amount of self-feedback versus cross-feedback. This allows the two optical modes to couple via the external cavity, that is, via the feedback. Indeed one would expect in general to observe a certain amount of cross-feedback. In Refs. [5,6] we showed that the case of purely self-feedback is degenerate. In this paper, for a general value of $\eta = 0.5$, we concentrate on the effect of the feedback phase C_p,

We briefly note that mathematically Eqs. (5)–(7) are delay differential equations (DDEs) with an infinite dimensional phase-space.[12] In particular, this means that stability calculations are much more involved than for the non-delayed case; DDEs have stability spectra consisting of infinitely many eigenvalues.[12] However, from a computational point of view, tools are available with which to analyse the stability of such systems.[7,8] In Ref. [5], when analysing the ECMs of a 105-dimensional derivation of our VCSEL model obtained by using a second-order finite difference scheme, we pushed these tools to their limits (with respect to computational time and, more importantly, memory usage). The advantage of the eigenfunction expanded 18-dimensional model (5)–(7) is that we can now use advanced tools to perform a multi-parameter bifurcation analysis, where we can even include studies of bifurcating periodic solutions.[6] As a direct comparison, stability computations of an ECM in the 105-dimensional model take 70 times as long as the same computation in the 18-dimensional model.

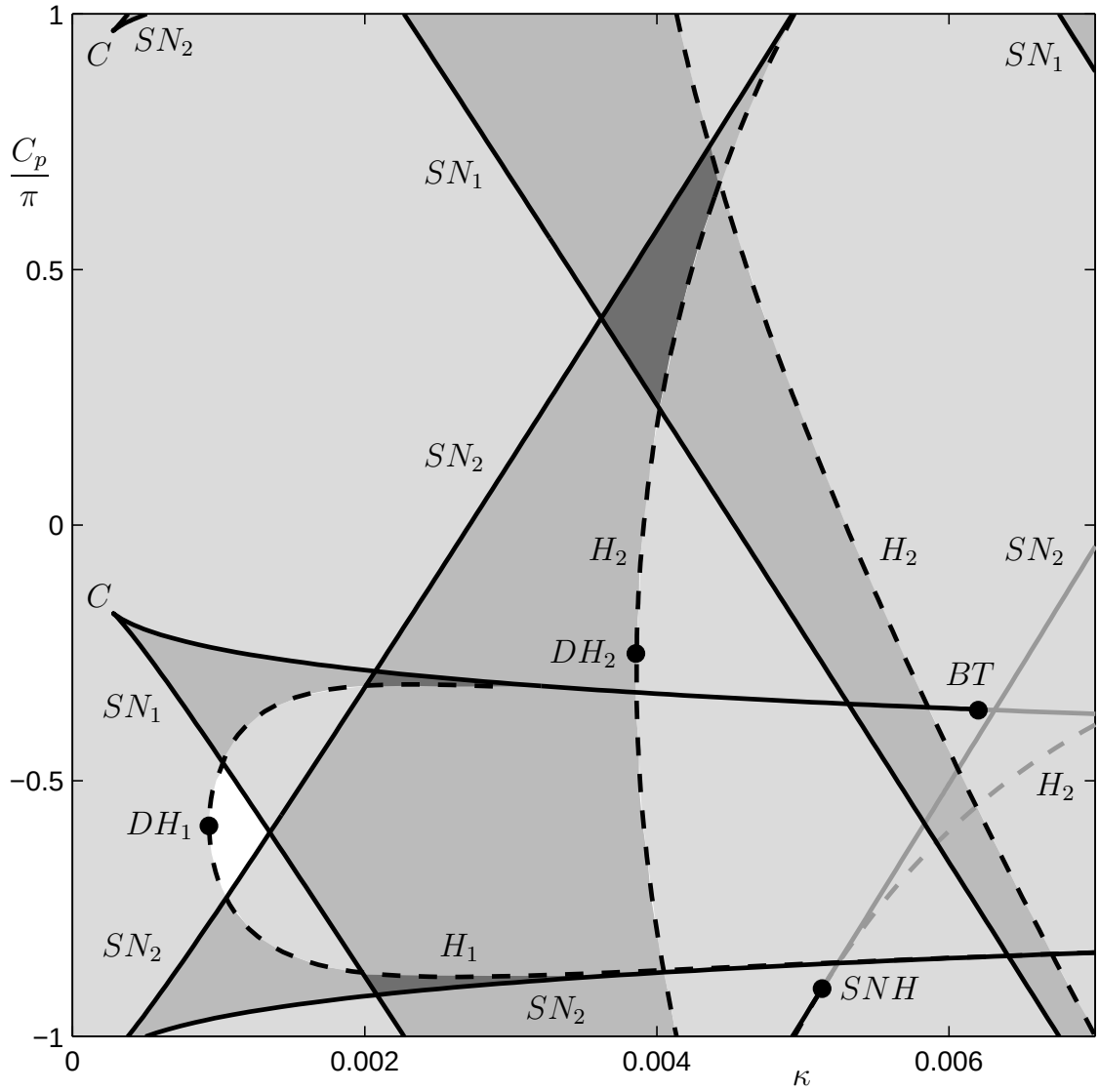

Figure 2. Two parameter bifurcation diagrams showing the power of the feedback strength κ against the feedback phase C_p, for fixed cross-coupling $\eta = 0.5$. Solid curves correspond to saddle-node bifurcations SN and dashed curves to Hopf bifurcations H. Shaded areas correspond to regions of coexisting stable ECMs.

3. BIFURCATION ANALYSIS

In this section, we study the stability and bifurcations of the basic steady state solutions of the VCSEL subject to optical feedback. Namely, the constant intensity, fixed frequency *external cavity modes* (ECMs). These solutions are given by

$$(E_1(t), E_2(t), N(t)_{1\ldots14}) = (R_1 e^{i\omega_s t}, R_2 e^{i\omega_s t + i\Phi}, N^s_{1\ldots14}), \tag{11}$$

where $R_1, R_2, \omega_s, N^s_{1\ldots14} \in \mathbb{R}$. The ECMs reflect the fundamental S^1-symmetry of Eqs. (5)–(7), a common feature of most laser systems subject to optical feedback.[13] Note also the 2π-periodicity of the feedback phase parameter C_p. In what follows, we will study the stability and bifurcations of these ECMs by using the continuation package `DDE-BIFTOOL`.[7] Parameters were fixed to those values given in Sec. 2, in particular, we fix the cross-coupling parameter to $\eta = 0.5$. This value was chosen because it is representative for the stability and bifurcations of the ECMs over a large range of intermediate values of cross-coupling.[6]

Figure 2 shows regions of ECM stability and their bifurcations in the two-parameter (κ, C_p)-plane. The degree of shading corresponds to regions in which one finds an increasing number of stable ECMs (in the white area there are no stable ECMs). These regions are bounded by curves of saddle-node bifurcations SN (drawn as solid curves) and Hopf bifurcations H (drawn as dashed curves). Supercritical bifurcations are black and subcritical are grey; that is, these bifurcations give rise to stable or unstable solutions, respectively. Again, we recall the 2π-periodicity of C_p; that is, curves that leave the lower boundary of Fig. 2, at $C_p = -\pi$, re-enter at the upper boundary, $C_p = \pi$ (observe the labelling of the curves).

The bifurcations shown in Fig. 2 are representative for a generic, non-zero range of the cross-coupling around $\eta = 0.5$. For fixed values of C_p, as κ is increased it is clear that stable ECMs are born in supercritical saddle-node bifurcations. These solutions are destabilised in subsequent supercritical Hopf bifurcations. From Fig. 2, it is clear that a single, stable ECM is born at $\kappa = 0$. Moreover, the value of C_p is seen to have a strong effect on the stability of ECMs. In particular, in the region surrounding $(\kappa, C_p) \approx (0.001, (-0.6 + 2n)\pi)$ $(n \in \mathbb{Z})$ one finds no stable ECMs; the stable ECM born at $\kappa = 0$ is destabilised in the Hopf curve H_1. In the case of a single-mode laser, this lack of stable solution above threshold has been contributed to negative interference between the outgoing and reflected fields for $C_p = (2n + 1)\pi$.[14] In our case, we find this zero solution slightly away from these values of C_p, which is most likely a result of the multi-mode interaction. The saddle-node curves SN_1 and SN_2, which give rise to the regions of multistability for low values of κ, appear from codimension-two cusp points C at $(\kappa, C_p) \approx (2.8 \times 10^{-4}, (-0.17 + 2n)\pi)$ and $(\kappa, C_p) \approx (2.8 \times 10^{-4}, (0.97 + 2n)\pi)$. As such, for values of $C_p \in [(-1.03 + 2n)\pi, (-0.17 + 2n)\pi]$ additional stable ECMs are born for much lower values of κ than for $C_p \in [(-0.17 + 2n)\pi, (0.97 + 2n)\pi]$. The Hopf curves H_1 and H_2 are clearly defined in terms of being born at low and high values of κ, respectively. In Ref. [6] it was shown that these Hopf bifurcations can give rise to two distinct types of periodic solution. Namely, high frequency, in-phase ROs (associated with the frequency of an undamped relaxation oscillation) and low frequency, anti-phase EOs (associated with the external cavity round-trip frequency). The Hopf curve H_1 is responsible for EOs, and the Hopf curve H_2 for ROs. Furthermore, at the leftmost turning point of both Hopf curves one finds codimension-two double Hopf points DH. Such a bifurcation point can give rise to torus bifurcations, which physically result in quasiperiodic modulation of the laser light. Two further codimension-two points are identified in Fig. 2 by large dots: a Bogdanov-Takens point BT and a saddle-node Hopf point SNH. The first point can again give rise to torus bifurcations and the latter to homoclinic bifurcations.[6,15]

The regions of differing stability identified in Fig. 2 are re-emphasised in Fig. 3 where we show one-parameter branches of ECMs for different values of κ. Specifically, from Fig. 3(a) to (i), we plot the power of the first field P_1 against the feedback phase C_p for fixed $\kappa = 0.0$, 0.0001, 0.001, 0.002, 0.003, 0.004, 0.005, 0.006 and 0.007, respectively. Parts of the branches on which one finds stable ECMs are drawn black; parts on which one finds unstable ECMs are drawn in grey. Saddle-node bifurcations are indicated by a '$\times$'; it is already clear that these occur at turning points of the branches, with respect to C_p. Hopf bifurcations are indicated by a '$*$'. (Note that we now plot all subcritical Hopf bifurcations; that is, some that are not included in Fig. 2.) For zero feedback Fig. 3(a) shows that one finds a single solution at a constant power for all values of C_p; this is the solution corresponding to the solitary/free-running laser solution. As κ is increased from zero, a stable ECM solution is born. For $\kappa = 0.0001$, Fig. 3(b) shows that this solution is stable for all values of C_p; compare with Fig. 2. Figure 3(c), for $\kappa = 0.001$, shows the emergence of saddle-node ($\times$) and Hopf ($*$) bifurcations. More specifically, a pair of saddle-node bifurcations appear for large values of P_1. These appear from the cusp bifurcation C identified in Fig. 2. The emergence of these saddle-node bifurcations causes the one-parameter branch of ECMs shown in Fig. 3(c) to fold over on itself. This results in values of C_p at which one finds bistability between ECMs, indicated by the slightly darker regions of Fig. 2 directly to the right of the cusp points C. Moreover, a pair of Hopf bifurcations is seen to be born for low values of P_1. These emerge from a double Hopf bifurcation, marked DH_1 in Fig. 2. Between these Hopf bifurcations one finds values of C_p for which there are no stable ECMs, also identified in Fig. 2. As κ is increased further, the 'loops' in these branches are seen to pass through one another and expand in C_p; see Figs. 3(d) to (i). This results in an ever increasing coexistence between ECMs for fixed values of C_p. Moreover, stable parts of the branches start overlapping and, thus, the region with no stable ECMs is destroyed. Note that this can be seen by the crossings of the saddle-node bifurcation curves SN_1 and SN_2 in Fig. 2. However, these crossings do not correspond to codimension-two bifurcations as it is clear that they do not occur on the same parts of the one-parameter branches shown in Fig. 3. Finally, in Figs. 3(g)

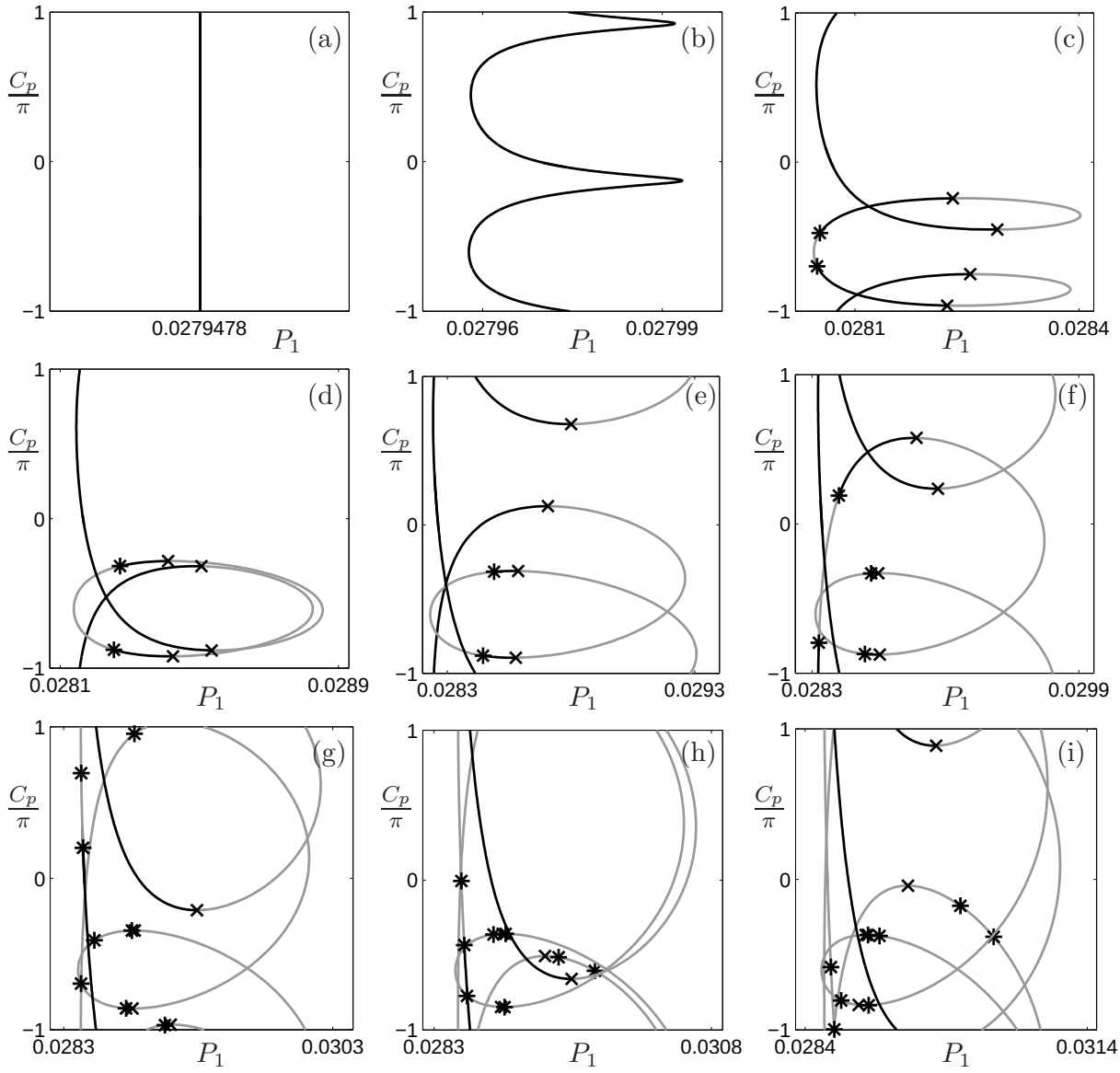

Figure 3. One-parameter bifurcation diagrams showing the power of the first field P_1 against the feedback phase C_p. Parts of the branch containing stable ECMs are drawn in black; unstable are drawn in grey. Saddle-node bifurcations are marked by a '×'; Hopf bifurcations by a '∗'. From (a) to (i), the feedback strength takes the values $\kappa = 0.0$, 0.0001, 0.001, 0.002, 0.003, 0.004, 0.005, 0.006 and 0.007, respectively.

to (i) the emergence of the codimension-two saddle-node Hopf points, and Bogdanov-Takens point, are clearly observed by the saddle-node and Hopf points coming together at the same point along the branches of ECMs; for example, follow the shrinking region of stability between Hopf and saddle-node bifurcations from Fig. 3(c) to (g). We note that these codimension-two points give rise to bifurcations of the periodic solutions emanating from the Hopf bifurcations. We finish this study by showing some simulation results relating to these solutions.

4. TRANSITIONS TO MORE COMPLICATED DYNAMICS

Figures 4 and 5 show the attracting dynamics for two different bifurcation scenarios corresponding to the ROs and EOs; recall that these solutions emanate from the respective Hopf curves H_2 and H_1 of Fig. 2. In each figure, the top row shows the stable attractor for each field (the first in black, the second in grey) in projection

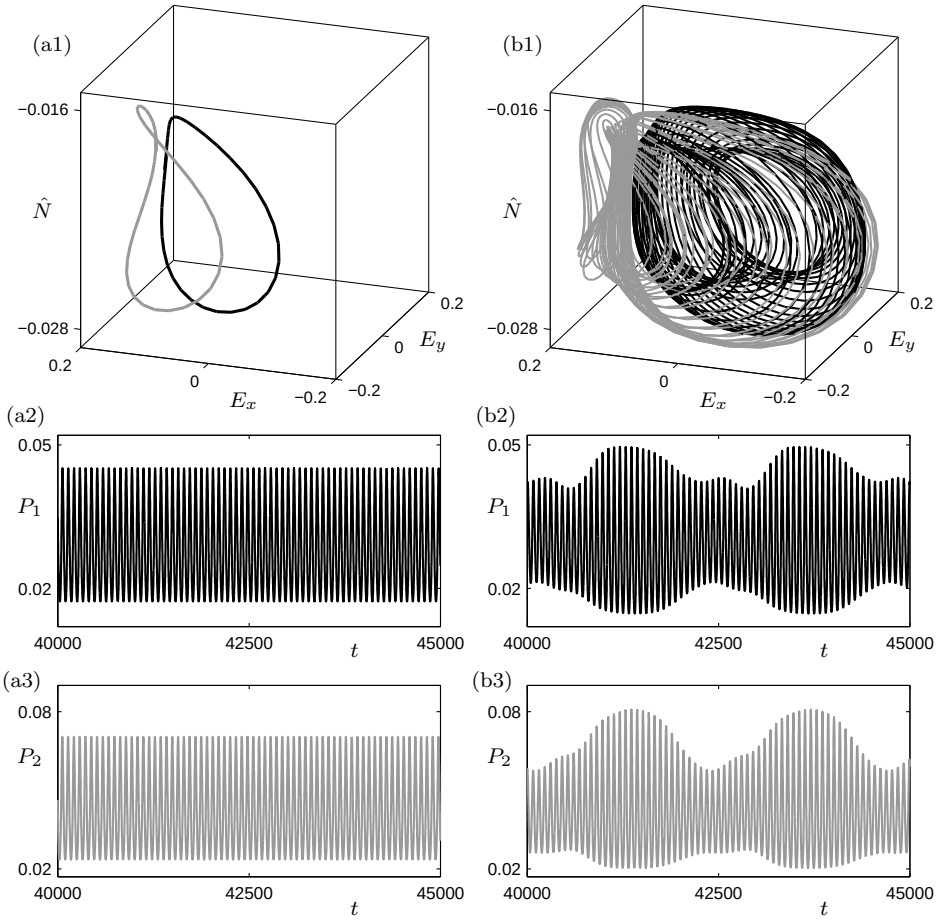

Figure 4. From periodic to quasiperiodic modulations. For (a) and (b) κ takes the values 0.0054 and 0.0062, respectively; for fixed $\eta = 0.5$ and $C_p = 0.0$. The first row shows projections of the dynamics of each optical field into $(E_x, E_y, \hat{N})$-space, where E_x and E_y are the real and imaginary parts of the electric field, and $\hat{N}$ is the mean of the inversion expansion coefficients. The lower two rows show the temporal evolution of the in-phase dynamics of each of the two fields.

into $(E_x, E_y, \hat{N})$-space, where E_x and E_y are the real and imaginary parts of each electric field, and $\hat{N}$ is the mean of the 14 inversion expansion coefficients. The lower two rows show the temporal evolution of the powers $P_1 = |E_1|^2$ (in black) and $P_2 = |E_2|^2$ (in grey) of the two optical fields. Our first observation is that the dynamics shown in Fig. 4 take place over a much shorter timescale (have a much higher frequency) than those shown in Fig. 5. This demonstrates our distinction between ROs and EOs; the former operate on the fast timescale of undamped relaxation oscillations, while the latter follow the slower external cavity round-trip time.

More specifically, Fig. 4 shows the destabilisation of an in-phase RO through a torus bifurcation for $C_p = 0.0$. The in-phase behaviour of the RO shown in Fig. 4(a) for $\kappa = 0.0054$ is inherited by the bifurcating torus, shown in Fig. 4(b) for $\kappa = 0.0062$. Note that the emanating 'slow' frequency of this torus is approximately 500 time units: that of the external cavity round-trip time.

Figure 5 shows the break-up of an anti-phase EO in a period-doubling route to chaos for $C_p = -0.3\pi$. The anti-phase EO shown in Fig. 5(a) for $\kappa = 0.0018$ bifurcates into a period-two EO (shown in Fig. 5(b) for $\kappa = 0.002$); this period doubles to a period-four EO (shown in Fig. 5(c) for $\kappa = 0.00207$); after further period-doubling bifurcations an anti-phase chaotic attractor emerges (shown in Fig. 5(d) for $\kappa = 0.00219$). Observe that throughout this transition the anti-phase nature of the original EO is preserved.

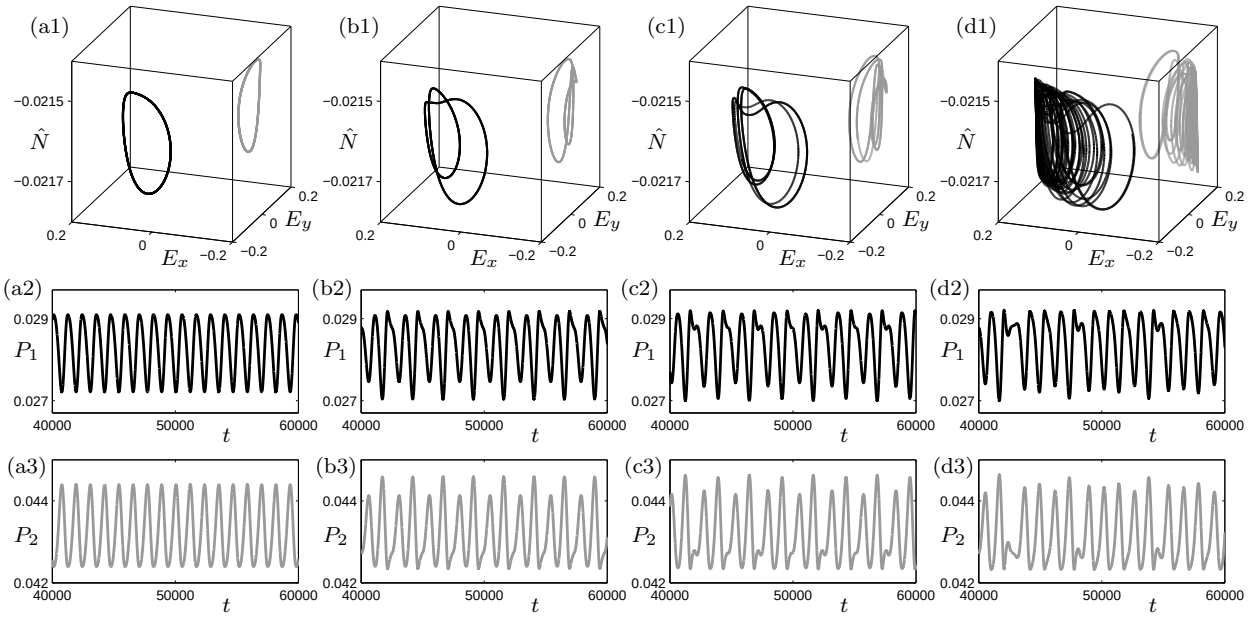

Figure 5. Period-doubling route to chaos. From (a) to (d), κ takes the values 0.0018, 0.002, 0.00207 and 0.00219, respectively; for fixed $\eta = 0.5$ and $C_p = -0.35\pi$. The first row shows projections of the the dynamics of each optical field into $(E_x, E_y, \hat{N})$-space, where E_x and E_y are the real and imaginary parts of the electric field, and $\hat{N}$ is the mean of the inversion expansion coefficients. The lower two rows show the temporal evolution of the anti-phase dynamics of each of the two fields.

5. CONCLUSIONS

We have presented a two-parameter bifurcation analysis of the steady states of a two-mode VCSEL subject to optical feedback. This approach was made possible by first resolving the spatial nature of the problem to arrive at a relatively small system of DDEs. Furthermore, we formulated the feedback term such that the two modes couple in the external round-trip. Our analysis revealed a number of regions in which one finds coexisting stable ECMs. These solutions were shown to be born in saddle-node bifurcations and destabilised in Hopf bifurcations, in which periodic solutions are born. The interaction of curves of these codimension-one bifurcations identified a number of codimension-two bifurcation points: double-Hopf and Bogdanov-Takens points that lead to subsequent torus bifurcations of the periodic solutions, and a saddle-node Hopf bifurcation point that can lead to low frequency, homoclinic dynamics.[6]

The Hopf curves were categorised as those resulting in high frequency periodic oscillations ROs (on the frequency of undamped relaxation oscillations) and much lower frequency EOs (on the frequency of the external-cavity round-trip time). The EOs were found close to the saddle-node Hopf point; the point of low frequency homoclinic dynamics. We went on to show how ROs and EOs undergo characteristic instabilities. Namely, the ROs were shown to destabilise in a torus bifurcation (again, a consequence of nearby double-Hopf points) and the EOs in a period-doubling route to chaos (typical for nearby homoclinic bifurcations).

We conjecture that the slower EOs (and their bifurcating solutions) are due to a much stronger competition between the two optical fields over the same reservoir of carriers. Indeed, the two fields exhibiting EOs are much closer to one another in both state space and in amplitude than the RO fields. This could also be a result of their anti-phase character; that is, the weakening of one field allows the other a chance to fully develop and vice versa. Finally, we believe that observation of a clear difference between EOs and ROs could be a way of determining the amount of cross-feedback between multi-mode VCSELs in an experiment. This would require two-parameter analyses for a number of values of η, which is work for the future.

ACKNOWLEDGMENTS

K. G. is funded by the Dynamics of Patterns Program of the Netherlands Organisation for Scientific Research (NWO) and the Foundation for Fundamental Research on Matter (FOM).

REFERENCES

[1] Chong, C. H. and Sarma, J., "Lasing Mode Selection in Vertical-Cavity Surface-Emitting Lasers" IEEE Photon. Tech. Lett. **5**, 761–764 (2003).

[2] Dellunde, J., Valle, A. and Shore, K. A., "Transverse-mode selection in external-cavity vertical-cavity surface-emitting laser diodes", J. Opt. Soc. Am. B **13**, 2477–2483 (1996).

[3] Valle, A., "Selection and modulation of high-order transverse modes in vertical-cavity surface-emitting lasers", IEEE J. Quantum Electron. **34**, 1924–1932 (1998).

[4] Yu, S. F., [Analysis and Design of Vertical Cavity Surface Emitting Lasers], Wiley (2003).

[5] Green, K., Krauskopf, B. and Lenstra, D., "External cavity mode structure of a two-mode VCSEL subject to optical feedback" Opt. Commun. **277**, 359–371 (2007).

[6] Green, K., Krauskopf, B., Marten, F. and Lenstra, D., "Bifurcation analysis of a spatially extended laser with optical feedback", Preprint (2008). `http://rose.bris.ac.uk/dspace/handle/1983/1013`

[7] Engelborghs, K., Luzyanina, T., Samaey, G. and Roose, D., "DDE-BIFTOOL: a Matlab package for bifurcation analysis of delay differential equations", Tech. Rep. TW-330, Department of Computer Science, K. U. Leuven, Belgium (2001). `http://www.cs.kuleuven.ac.be/cwis/research/twr/research/software/delay/ddebiftool.shtml`.

[8] Szalai, R., "PDDE-CONT: A continuation and bifurcation software for delay-differential equations", Budapest University of Technology and Economics, Hungary (2005). `http://www.mm.bme.hu/~szalai/pdde`

[9] Torre, M. S., Masoller, C., and Mandel, P., "Transverse-mode dynamics in vertical-cavity surface-emitting lasers with optical feedback", Phys. Rev. A **66**:053817 (2002).

[10] Onishi, Y., Nishiyama, N., Caneau, C., Koyama, F. and Zah, C.-E., "All-Optical Regeneration Using Transverse Mode Switching in Long-Wavelength Vertical-Cavity Surface-Emitting Lasers", Jap. J. Appl. Phys. **45**, 467–468 (2006).

[11] Lang,R., and Kobayashi, K., "External optical feedback effects on semiconductor injection laser properties", IEEE J. Quantum Electron. **16**(3), 347–355 (1980).

[12] Hale, J. K. and Verduyn Lunel, S. M., [Introduction to Functional Differential Equations], Springer-Verlag (1993).

[13] Krauskopf, B., van Tartwijk, G. H. M. and Gray, G. R., "Symmetry properties of lasers subject to optical feedback", Opt. Commun. **177**, 347–353 (2000).

[14] Rottschäfer, V. and Krauskopf, B., "The ECM-backbone of the Lang-Kobayashi equations: A geometric picture", Int. J. Bif. and Chaos **17**(5), 1575–1588 (2007).

[15] Kuznetsov, Yu., [Elements of Applied Bifurcation Theory], Third Edition, Springer-Verlag (2004).